

ISSN Online: 2151-4844 ISSN Print: 2151-481X

# Impact of the Doping Rate of Different Zone of the Bifacial PV Cell on the Electrical Parameters

Ramatou Konate<sup>1,2\*</sup>, Bernard Zouma<sup>1</sup>, Bruno Korgo<sup>1</sup>, Aboubacar Savadogo<sup>1</sup>, Cyrile Constant Moyenga<sup>1</sup>, Issa Zerbo<sup>1</sup>

<sup>1</sup>Département de Physique, Laboratoire d'Energies Thermiques Renouvelables (L. E. T. RE) Université Joseph KI-ZERBO, Ouagadougou, Burkina Faso

<sup>2</sup>Département de Physique, Université Virtuelle du Burkina Faso, Ouagadougou, Burkina Faso Email: \*ramatou.konate@uv.bf

How to cite this paper: Konate, R., Zouma, B., Korgo, B., Savadogo, A., Moyenga, C.C. and Zerbo, I. (2025) Impact of the Doping Rate of Different Zone of the Bifacial PV Cell on the Electrical Parameters. Smart Grid and Renewable Energy, 16, 187-202.

https://doi.org/10.4236/sgre.2025.1610011

Received: August 5, 2025 Accepted: October 28, 2025 Published: October 31, 2025

Copyright © 2025 by author(s) and Scientific Research Publishing Inc. This work is licensed under the Creative Commons Attribution International License (CC BY 4.0).

http://creativecommons.org/licenses/by/4.0/





#### **Abstract**

In this work, we investigate the effect of the doping rate on the electrical parameters of the different zones of the bifacial polycrystalline silicon solar cell under multispectral illumination. To do this, from our hypothesis, we determined the expression of the continuity equation in the emitter, the base and the overdoped zone  $p^+$ . The photocurrent density, photovoltage and electrical power were studied as a function of the dynamic velocity at the junction for different values of the doping rate. The results obtained by simulation show us that to achieve the best performance of the bifacial PV cell the doping rate of the emitter should be between  $[10^{18} - 10^{19} \, \text{cm}^{-3}]$ , that of the base between  $[10^{16} - 10^{17} \, \text{cm}^{-3}]$  and for the  $p^+$  zone between  $[10^{20} - 10^{21} \, \text{cm}^{-3}]$ . Within these doping ranges, the fill factor, which represents the efficiency of the cell, reaches optimal values.

## **Keywords**

Doping Rate, Base, Emitter, p<sup>+</sup> Overdoped Zone, Bifacial Solar Cell

#### 1. Introduction

Improving the performance of PV cells is a major concern towards which current research is turning. This improvement is obtained by optimizing various parameters [1]-[3]. Among these parameters, is doping which ensures the movement of charge carriers from one zone to another (base and emitter) through the electric field created at the junction. Indeed, doping silicon consists of introducing impurities into it. These impurities are atoms which will replace other silicon atoms, they are classified into two categories: donor and acceptor atoms. Depending on

whether the replacing atom has one more electron than silicon on its valence layer, it is called a donor, otherwise it is called an acceptor. Thus, the silicon doped by donor atoms is of type N, constitutes the emitter of the PV cell, that doped by acceptor atoms is of type P, constitutes the base of the PV cell and the p<sup>+</sup> overdoped part at the back of the base. Doping is therefore fundamental for the operation of the PV cell whatever its type. Our objective is to carry out a study of the impact of the doping rate on different zones of the bifacial PV cell in a magnetic field under multispectral illumination. This involves determining the impact of the doping rate on the electrical parameters of the bifacial PV cell. This will lead to an identification of a range of doping rates of different zones on the performance of the bifacial PV cell. However, the resolution of the equations will be given in the methods and theories section. The effect of the doping rate of the emitter, the base and the  $p^+$  zone on the photocurrent density (J), the photovoltage (V), the electrical power (P) and the fill factor (FF) of the bifacial polycrystalline silicon PV cell for simultaneous illumination on both sides will be presented in the results section. Conclusions will be drawn at the end of this work.

# 2. Methods and Theory

## **Assumptions and Basic Equations**

The model of this study is a three-dimensional (3D) grain extracted from a bifacial polycrystalline silicon PV cell. It mainly includes three parts: the emitter, the base and the  $p^+$  overdoped zone equipped with an active surface for albedo collection.

**Figure 1** illustrates the three-dimensional structure of a bifacial photovoltaic cell at the grain scale. The device is composed of three successive regions: the emitter  $(-W \le z \le 0)$ , the base  $(0 \le z \le H)$ , and the heavily doped  $p^+$  layer  $(H \le z \le H + W_{bst})$ .

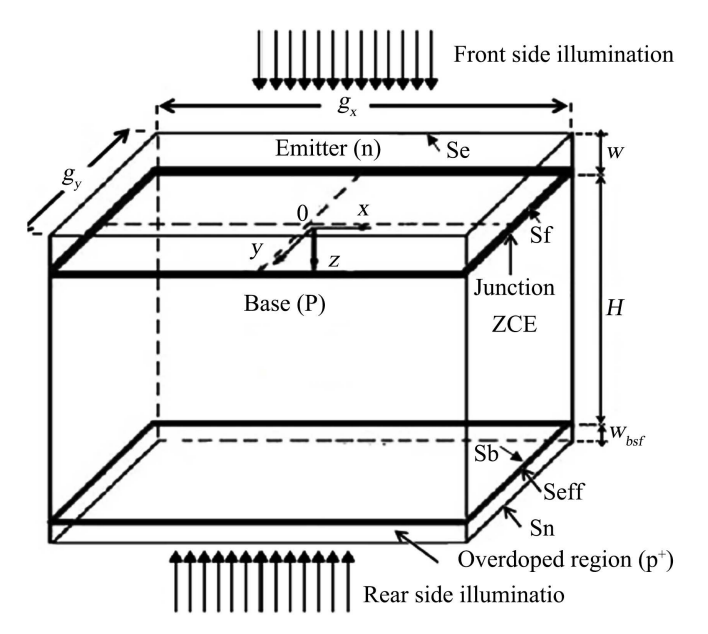


Figure 1. Three-dimensional model of a bifacial PV cell grain [3].

To simplify the formulation and solution of the governing equations, the following assumptions are made: The excess minority carrier generation is assumed to occur only along the (OZ) direction, which is perpendicular to the junction. The electric field is confined within the space charge region (SCR) [4]. The parameters W, H, and  $W_{bsf}$  represent the thicknesses of the emitter, the base, and the overdoped layer, respectively. Finally,  $g_x$  and  $g_y$  denote the grain dimensions along the x and y axes, which define the flat surface exposed to incident light.

- The grain boundaries are positioned at  $x = \pm \frac{g_x}{2}$  and  $y = \pm \frac{g_y}{2}$ , with the origin taken at the center of the top surface [4].
- Under thermodynamic equilibrium, the emitter, base, and P<sup>+</sup> regions are considered quasineutral. No internal electric field exists in these regions, which justifies the use of Cartesian coordinates.
- The influence of magnetic field-induced border effects is neglected. In principle, such effects would arise from charge accumulation on the lateral faces of the grain due to the Hall effect, but they are assumed to be insignificant here. The grain's top surface is taken as square, *i.e.*,  $g_x = g_y$ .
- The shading of the front and rear collecting grids is included in the model. However, only the reflection from the silicon material itself is considered, since the external surfaces of the cell are coated with an anti-reflective layer. The effect of temperature on cell performance is neglected.

The three-dimensional continuity equations in the steady-state regime, describing the base, the  $p^+$  region, and the emitter, are derived from the magnetotransport equations under multispectral illumination [5].

· In the base

$$\frac{\partial^2 \delta_n}{\partial x^2} + \frac{\partial^2 \delta_n}{\partial y^2} + \frac{\partial^2 \delta_n}{\partial z^2} - \frac{\delta_n}{\tau_n D_n^*} + \frac{G(z)}{D_n^*} = 0$$
 (1)

In the overdoped p<sup>+</sup> zone

$$\frac{\partial^{2} \delta_{n^{+}}}{\partial x^{2}} + \frac{\partial^{2} \delta_{n^{+}}}{\partial y^{2}} + \frac{\partial^{2} \delta_{n^{+}}}{\partial z^{2}} - \frac{\partial_{n^{+}}}{L_{+}^{*}} + \frac{G(z)}{D_{+}^{*}} = 0$$
 (2)

• In the emitter

$$\frac{\partial^2 \delta_p}{\partial x^2} + \frac{\partial^2 \delta_p}{\partial y^2} + \frac{\partial^2 \delta_p}{\partial z^2} - \frac{\delta_p}{\tau_p D_p^*} + \frac{G(z)}{D_p^*} = 0$$
 (3)

The expression of the generation rate, G(z), is given in [6].

- Simultaneous illumination on both faces

$$G(z) = n \sum_{m=1}^{3} a_m \left[ e^{-b_m[W+z]} + e^{-b_m[H+W_{bsf}-z]} \right]$$
 (4)

The coefficients  $a_m$  and  $b_m$  are determined from tabulated solar irradiance data [7] [8]. These coefficients are given for an AM 1.5 solar spectrum by:

$a_1$	$a_2$	$a_3$	$b_1$	$b_2$	$b_3$
$6.13 \times 10^{20}$	$0.54\times10^{20}$	$0.991 \times 10^{20}$	6630	1000	130

The parameter n, commonly referred to as the number of suns, represents the concentration factor of the incident solar radiation.

### 3. Excess Minority Charge Carrier Densities

In the base region, the excess minority carriers are electrons; in the  $p^+$  region, they are also electrons; whereas in the emitter, the excess minority carriers are holes. This subsection also presents the dependence of the diffusion coefficients and carrier lifetimes on the doping concentration. In the base, the diffusion coefficient and carrier lifetime are defined according to Liou *et al.* [9]:

$$D_n(N_b) = 1350V_t \frac{1}{\sqrt{1 + \frac{81N_b}{N_b + 3.2 \times 10^{18}}}}$$
 (5)

$$\tau_n(N_b) = \frac{1}{1 + \frac{N_b}{5 \times 10^{16}}} \tag{6}$$

Here,  $N_b$  denotes the doping concentration of the base, and  $V_t$  represents the thermal voltage.

In the heavily doped  $p^+$  region, the diffusion coefficient and carrier lifetime are defined according to the formulation of S. E. Swirhun *et al.* [10].

$$D'(N_{bsf}) = V_{t} \left[ 232 + \frac{1180}{1 + \left(\frac{N_{bsf}}{8 \times 10^{16}}\right)^{0.9}} \right]$$
 (7)

$$\tau_n'(N_{bsf}) = \frac{1}{3.45 \times 10^{-12} N_{bsf} + 0.95 \times 10^{-31} N_{bsf}^2}$$
(8)

In the emitter, the diffusion coefficient and carrier lifetime are defined according to the model proposed by Bensmaïne *et al.* [11].

$$D_n(N_e) = 480V_t \frac{1}{\sqrt{1 + \frac{350N_e}{N_e + 1.05 \times 10^{19}}}}$$
(9)

$$\tau_p(N_e) = \frac{1}{7.8 \times 10^{-3} N_e + 1.8 \times 10^{-31} N_e^2}$$
 (10)

The governing equation is a second-order differential equation with constant coefficients, and its solution is provided in [5].

$$\delta(x, y, z) = \sum_{j} \sum_{k} Z_{jk}(z) \cos(c_{j}x) \cos\left(\frac{c_{k}}{\theta}y\right)$$
 (11)

#### 4. Determination of Electrical Parameters

To evaluate the electrical parameters, we consider a bifacial photocell grain with a square surface of side 0.01 cm ( $g_x = g_y = 0.01$ , cm). The surface recombination velocity at the grain boundaries is assumed identical for both the base and the

emitter, with  $S_g = 100$ , cm·s<sup>-1</sup>. The layer thicknesses are set as follows: 100,  $\mu$ m for the base, 0.1,  $\mu$ m for the p<sup>+</sup> region, and 0.1,  $\mu$ m for the emitter [12].

#### 4.1. Photocurrent Density

Define The electron and hole photocurrent densities depend on the gradients of the excess minority carriers [13]. Under simultaneous illumination on both sides, the photocurrent density in the emitter is expressed as follows:

$$J_{p}\left(S_{f}, N_{b}\right) = -eD_{p} \sum_{j=0}^{\infty} \sum_{k=0}^{\infty} S_{pjk} \left[ \frac{B_{pjk}}{L_{pjk}^{*}} + \sum_{m=1}^{3} b_{m} T_{pjk} \left[ e^{-b_{m}W} - e^{-b_{m}\left[H + W_{b,sf}\right]} \right] \right]$$
(12)

Under simultaneous illumination on both faces, the photocurrent density in the base is given by:

$$J_{n}(S_{f}, N_{b}) = eD_{n} \sum_{j=0}^{\infty} \sum_{k=0}^{\infty} S_{njk} \left[ \frac{B_{njk}}{L_{nik}^{*}} + \sum_{m=1}^{3} b_{m} T_{njk} \left[ e^{-b_{m}W} - e^{-b_{m}[H + W_{bsf}]} \right] \right]$$
(13)

Under simultaneous illumination on both faces, the photocurrent density in the overdoped  $(p^+)$  region is expressed as:

$$J_{n^{+}}\left(S_{f}, N_{bsf}\right)$$

$$= eD_{n^{+}}^{*} \sum_{j=0}^{\infty} \sum_{k=0}^{\infty} S_{n^{+}jk} \left[ \frac{A_{n^{+}jk} + B_{n^{+}jk}}{L_{n^{+}jk}} + \sum_{m=1}^{3} b_{m} T_{n^{+}jk} \left[ e^{-b_{m}[W+H]} - e^{-b_{m}[W_{bsf}]} \right] \right]$$
(14)

# 4.2. Photovoltage

The voltage at the terminals of the photovoltaic cell under illumination is calculated using the Boltzmann relation [14].

For simultaneous illumination on both faces, the photovoltage in the base is given by the following equation:

$$V_{php}\left(S_f, N_e\right) = V_T \ln \left(1 + \frac{1}{n_0} * \sum_{j=0}^{\infty} \sum_{k=0}^{\infty} S_{p'jk} \left(A_{pjk} - \sum_{m=1}^{3} T_{pjk} \left[e^{-b_m W} + e^{-b_m \left(H + W_{bsf}\right)}\right]\right)\right)$$
(15)

Under simultaneous illumination on both sides, the photovoltage in the base is expressed as follows:

$$V_{phn}\left(S_{f}, N_{b}\right) = V_{T} \ln \left(1 + \frac{1}{n_{0}} * \sum_{j=0}^{\infty} \sum_{k=0}^{\infty} S_{n'jk} \left(A_{njk} - \sum_{m=1}^{3} T_{njk} \left[e^{-b_{m}W} + e^{-b_{m}(H + W_{bsf})}\right]\right)\right)$$
(16)

For simultaneous illumination on both faces, the photovoltage in the overdoped zone is evaluated using Equation (17).

$$V_{phn^{+}}\left(S_{f}, N_{bsf}\right) = V_{T} \ln \left(1 + \frac{1}{n_{0}} * \sum_{j=0}^{\infty} \sum_{k=0}^{\infty} \left(Z_{n^{+}jk}\left(H\right)\right) S_{n^{+}jk}\right)$$
(17)

#### 4.3. Electrical Power

The electrical power produced by the PV cell is given in emitter, base and the overdoped zone by the Equations (18), (19) and (20)

$$P_{p}\left(S_{f}, N_{e}\right) = J_{php} * V_{php} \tag{18}$$

$$P_n\left(S_f, N_b\right) = J_{phn} * V_{phn} \tag{19}$$

$$P_{n^{+}}(S_{f}, N_{bsf}) = J_{phn^{+}} * V_{phn^{+}}$$
(20)

#### 4.4. Determination of Fill Factor of the PV Cell

The fill factor defines the efficiency of the PV cell; it can also provide information on the aging of the PV cell. It is the ratio between the maximum power delivered and the ideal power [15]. For simultaneous illumination, the fill factor is given the electrical power produced by the PV cell is given in emitter, base and the overdoped zone by the Equations (21), (22) and (23).

$$FF_{p}\left(S_{f}, N_{e}\right) = \frac{J_{php \max} * V_{php \max}}{J_{phcc} * V_{phco}} \tag{21}$$

$$FF_{n}\left(S_{f}, N_{b}\right) = \frac{J_{phn \max} * V_{phn \max}}{J_{phcc} * V_{phco}}$$
(22)

$$FF_{n^{+}}(S_f, N_{bsf}) = \frac{J_{phn^{+}\max} * V_{phn^{+}\max}}{J_{phcc} * V_{phco}}$$
(23)

The determination of intrinsic parameters, namely diffusion coefficients, lifetimes and densities of excess minority charge carriers in addition to the evaluation of extrinsic parameters such as photovoltage and photocurrent density, electrical power and fill factor have been carried out in this section. In the following section the results and discussions of the influence of thickness on extrinsic parameters will be given.

#### 5. Results and Discussion

In this section, intrinsic parameters including diffusion coefficients, carrier lifetimes, and excess minority carrier densities have been determined, alongside the evaluation of extrinsic parameters such as photovoltage, photocurrent density, electrical power, and fill factor. In the following section, the results and discussion on the influence of layer thickness on these extrinsic parameters will be presented.

# **5.1. Impact of Doping Rate of the Emitter on the Photocurrent Density**

In this section, **Figure 2** presents the evolution of the photocurrent density as a function of the dynamic velocity at the junction for different Ne doping rates under simultaneous illumination of both faces.

In Figure 2, we observe a decrease in the photocurrent density for the values of  $S_f > 10^2$  cm·s<sup>-1</sup> when the doping rate of the emitter increases. But for a doping rate varying between  $10^{17}$  cm<sup>-3</sup> and  $10^{19}$  cm<sup>-3</sup>, this is very low. In short circuit, we observe a reduction in the photocurrent density of about 20.68% when the doping rate of the emitter goes from  $10^{17}$  cm<sup>-3</sup> to  $10^{21}$  cm<sup>-3</sup>. The increase in the doping

rate of the emitter leads to an increase in the electrons which are the majority carriers, the holes will be recombined and this will lead to a drop in the photocurrent density of the holes at the emitter. Indeed, the diffusion coefficient and the diffusion length both decrease with increasing  $N_e$  doping rate [2]. These two diffusion parameters are characteristic of the movements of charge carriers. The diffusion length is the distance traveled by the photogenerated charge carriers before recombining and the diffusion coefficient is related to the mobility of charge carriers. Hence the reduction in photocurrent density.

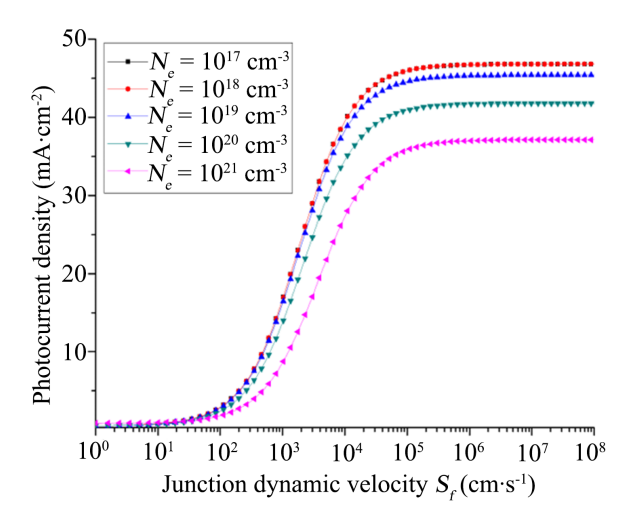


**Figure 2.** Photocurrent density as a function of dynamic velocity at the junction for different emitter doping rates ( $N_b = 10^{16} \text{ cm}^{-3}$ ,  $N_{bsf} = 10^{20} \text{ cm}^{-3}$ ,  $W = 0.1 \text{ }\mu\text{m}$ ,  $H = 100 \text{ }\mu\text{m}$ ,  $W_{bsf} = 0.1 \text{ }\mu\text{m}$ ).

#### 5.2. Impact of Doping Rate of the Emitter on Photovoltage

The evolution of the photovoltage as a function of the dynamic velocity at the junction for different doping rates of the emitter under simultaneous illumination of both faces is presented in **Figure 3**.

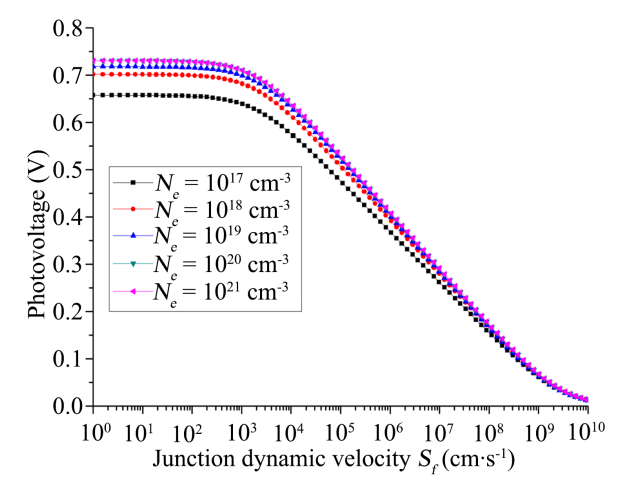


**Figure 3.** Photovoltage as a function of dynamic velocity at the junction for different emitter doping rates ( $N_b = 10^{16} \text{ cm}^{-3}$ ,  $N_{bsf} = 10^{20} \text{ cm}^{-3}$ ,  $W = 0.1 \text{ }\mu\text{m}$ ,  $H = 100 \text{ }\mu\text{m}$ ,  $W_{bsf} = 0.1 \text{ }\mu\text{m}$ ).

We notice that in open circuit, when the doping rate of the emitter increases from  $10^{17}$  cm<sup>-3</sup> to  $10^{21}$  cm<sup>-3</sup>, it appears an increase in the open circuit photovoltage of about 10%. Indeed, increasing.

The doping rate of the emitter leads to an increase in positive ions near the junction. the photovoltage being a difference of potentials will increase at the junction on the emitter side. This will cause an increase in the open circuit photovoltage. In the following part, we will determine the behavior of the electrical power as a function of the doping rate of the transmitter.

### 5.3. Impact of Doping Rate of the Emitter on Electrical

The figure below (**Figure 4**) represents the evolution of the electrical power as a function of the dynamic velocity at the junction for different doping rates of the  $N_c$  emitter under simultaneous illumination of both faces.

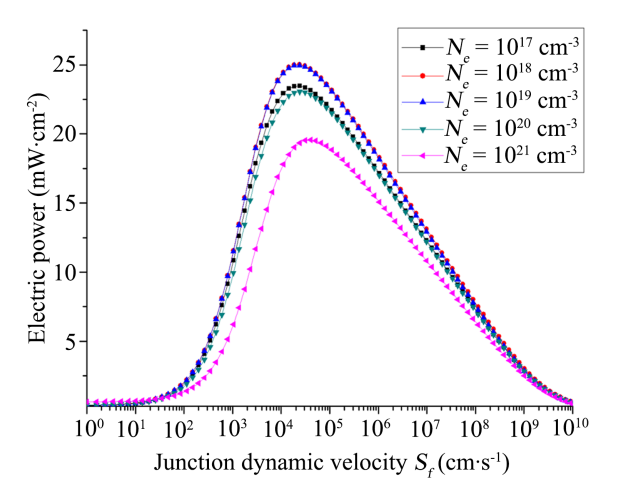


**Figure 4.** Electrical power as a function of dynamic velocity at the junction for different doping rates of the  $N_e$  emitter ( $N_b = 10^{16}$  cm<sup>-3</sup>,  $N_{bsf} = 10^{20}$  cm<sup>-3</sup>, W = 0.1 μm, H = 100 μm,  $W_{bsf} = 0.1$  μm).

We notice in this figure the impact of the doping rate of the transmitter on the maximum electrical power. We note that the maximum electrical power increases for the values of the doping rate  $10^{18}$  cm<sup>-3</sup> then decreases from this value. This state of affairs confirms the effect of the doping rate of the emitter  $N_c$  observed on the photocurrent density and the photovoltage. According to the results recorded in **Table 1**, we also notice that the very high doping rate acts negatively on the fill factor.

**Table 1.** Fill factor values as a function of doping rate  $N_e$ .

$N_e \left( \text{cm}^{-3} \right)$	$P_{\rm max} \left({\rm mW/cm^2}\right)$	$V_{co}\left(\mathrm{mV}\right)$	$J_{cc} \left( \text{mA/cm}^2 \right)$	FF (%)
1017	23.47	657.88	46.82	76.19
10 <sup>18</sup>	25.04	701.73	46.82	76.21
10 <sup>19</sup>	24.97	718.62	45.58	76.23

Continued				
10 <sup>20</sup>	23.06	730.95	41.80	75.47
$10^{21}$	19.36	730.95	37.14	71.31

As we can see, the fill factor increases when the doping rate  $N_e$  increases from  $10^{17}\,\mathrm{cm^{-3}}$  to  $10^{19}\,\mathrm{cm^{-3}}$  then decreases from  $10^{19}\,\mathrm{cm^{-3}}$ . The reduction in the fill factor is due to the fact that for the values of the doping rate  $N_e \leq 10^{19}\,\mathrm{cm^{-3}}$  the increase in the photovoltage com pensates for the short-circuit photocurrent losses. On the other hand, for  $N_e > 10^{19}\,\mathrm{cm^{-3}}$  the short circuit photocurrent loss becomes significant and can no longer be compensated by the open circuit photovoltage. Therefore, the doping rate  $N_e$  should be within the interval  $[10^{18}\,\mathrm{cm^{-3}}-10^{19}\,\mathrm{cm^{-3}}]$ . Subsequently, we will study the impact of the base doping rate.

## 5.4. Impact of the Base Doping Rate on Photocurrent Density

Figure 5 represents the evolution of the photocurrent density as a function of the dynamic velocity at the junction for different doping rates of the base under simultaneous illumination of the both faces.

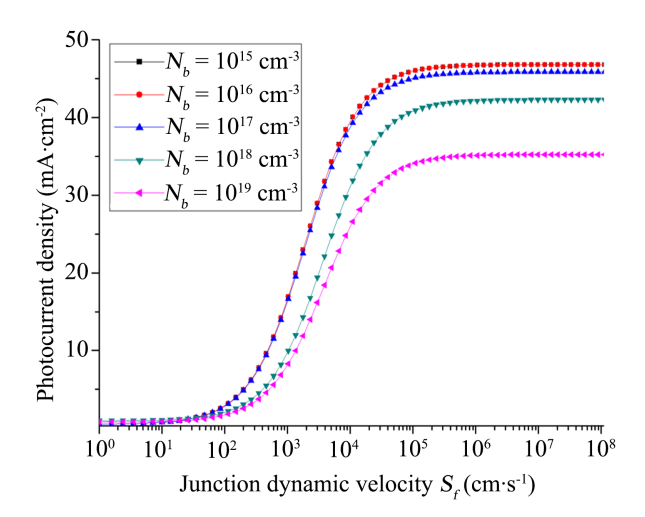


Figure 5. Photocurrent density as a function of dynamic velocity at the junction for different emitter doping rates. ( $N_e = 10^{19}$  cm<sup>-3</sup>,  $N_{bsf} = 10^{19}$  cm<sup>-3</sup>, W = 0.1 μm, H = 100 μm,  $W_{bsf} = 0.1$  μm).

We also notice that for the values  $S_f \le 10^2$  cm·s<sup>-1</sup> the doping rate of the base has no impact on the photocurrent density. On the other hand, for the values  $S_f > 10^2$  cm·s<sup>-1</sup> the short-circuit photocurrent density decreases when the doping rate of the base increases. In short circuit, this decrease in photocurrent density is about 24.67% when the base doping rate increases from  $10^{15}$  cm<sup>-3</sup> to  $10^{19}$  cm<sup>-3</sup>. Indeed, when the doping rate of the base is high, the holes which are the majority carriers increase. Consequently, very few electrons will be able to cross the junction to be collected and participate in the current of the short-circuited external circuit. Indeed, increasing the doping of the base leads to a reduction in the diffusion length

as well as the diffusion coefficient [2]. The electrons in the base of the PV cell will undergo significant recombination, hence the reduction in the short circuit photocurrent density. In the following section, we will study the impact of the doping rate of the base on the photovoltage.

#### 5.5. Impact of the Doping Rate of the Base on the Photovoltage

The study of the evolution of the photovoltage as a function of the dynamic velocity at the junction under simultaneous illumination of both faces, the curves obtained are presented in **Figure 6**.

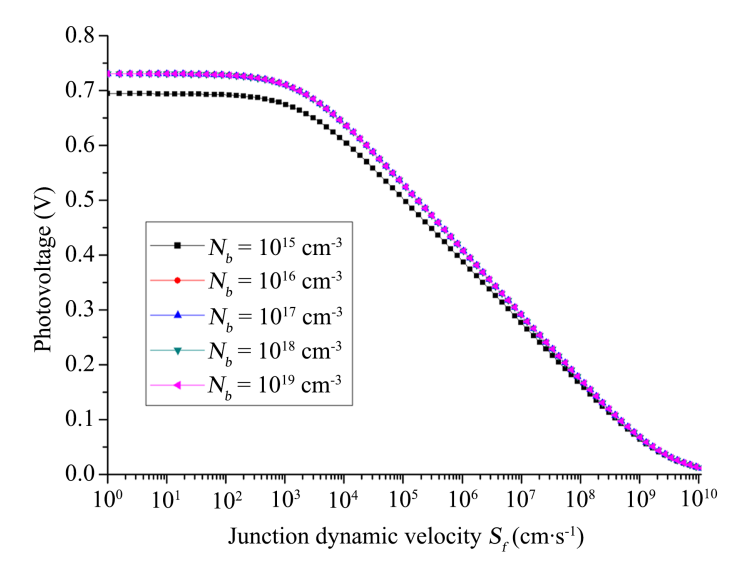


**Figure 6.** Photovoltage as a function of dynamic velocity for different base doping rates ( $N_e = 10^{19} \text{ cm}^{-3}$ ,  $N_{bsf} = 10^{19} \text{ cm}^{-3}$ ,  $W = 0.1 \text{ }\mu\text{m}$ ,  $H = 100 \text{ }\mu\text{m}$ ,  $W_{bsf} = 0.1 \text{ }\mu\text{m}$ ).

In short circuit, the photovoltage is very insensitive to variations in the doping rate of the base. On the other hand, in an open circuit the photovoltage increases by 5.23% when the doping rate of the base goes from  $10^{15}$  cm<sup>-3</sup> to  $10^{16}$  cm<sup>-3</sup> then remains constant from this base doping rate value.

Indeed, increasing the doping rate of the base leads to an increase in negative ions at the junction on the base side. Thus, the open circuit photovoltage which is a potential difference will increase. The electrons are then blocked in the base of the PV cell, resulting in an increase in the open circuit photovoltage despite the volume recombinations which increase with the doping rate of the base. Reason why the open circuit photovoltage increases when the doping rate of the base increases. In the following part, the evolution of the electrical power as a function of the doping rate of the base will be analyzed.

#### 5.6. Impact of Doping Rate of the Base on Electrical Power

**Figure 7** represents the evolution of the electrical power as a function of the dynamic velocity at the junction for different doping rates of the base under simultaneous illumination of the two faces.

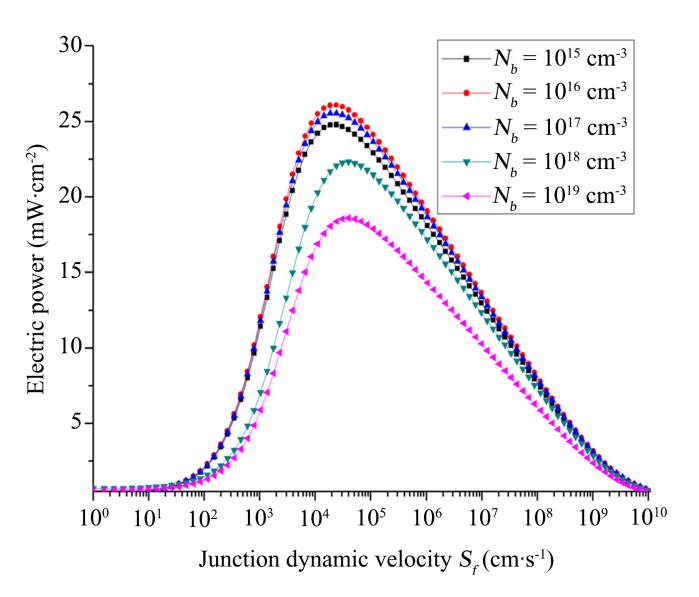


Figure 7. Electrical power as a function of dynamic velocity at the junction for different values of the base doping rate ( $N_e = 10^{19}$  cm<sup>-3</sup>,  $N_{bsf} = 10^{19}$  cm<sup>-3</sup>, W = 0.1 μm, H = 100 μm,  $W_{bsf} = 0.1$  μm).

The maximum electrical power increases for the values of the doping rate  $N_b \le 10^{16}$  cm<sup>-3</sup> then decreases for the values of the doping rate dopage  $N_b > 10^{16}$  cm<sup>-3</sup>. As the doping rate increases, the electrons in the base become less and less mobile, which favors their recombinations. This fact is linked to the decrease in the photocurrent density of the electrons observed previously. Which clearly justifies the reduction in electrical power when the doping rate of the base increases. We present, in **Table 2**, the values of the fill factor as a function of the doping rate of the base.

**Table 2.** Values of the fill factor as a function of the doping rate  $N_b$ .

$N_b \left( \text{cm}^{-3} \right)$	$P_{\rm max}\left({\rm mW/cm^2}\right)$	$V_{co}\left(\mathrm{mV}\right)$	$J_{cc}$ (mA/cm <sup>2</sup> )	<i>FF</i> (%)
10 <sup>15</sup>	24 .77	694.40	46.82	76.19
10 <sup>16</sup>	26.07	730.75	46.81	76.21
10 <sup>17</sup>	25.55	730.75	45.88	76.21
1018	22.05	730.75	42.23	71.45
10 <sup>19</sup>	18.37	730.75	35.27	71.27

We see that the fill factor undergoes a slight increase when the doping rate  $N_b$  goes from  $10^{15}$  cm<sup>-3</sup> to  $10^{16}$  cm<sup>-3</sup> then remains constant for the values of the doping rate between  $10^{16}$  cm<sup>-3</sup> and  $10^{17}$  cm<sup>-3</sup>. Then for values of  $N_b$  greater than  $10^{17}$  cm<sup>-3</sup> the fill factor decreases sharply. However, the optimal doping rate of the base must be between  $10^{16}$  cm<sup>-3</sup> and  $10^{17}$  cm<sup>-3</sup>. In the following part, the impact of the doping rate of the overdoped zone will be studied.

# 5.7. Impact of the Doping Rate of the Overdoped Zone on Photocurrent Density

Figure 8 shows the evolution of the photocurrent density as a function of the dynamic velocity at the junction for different doping rates of the overdoped zone under simultaneous illumination on both faces.

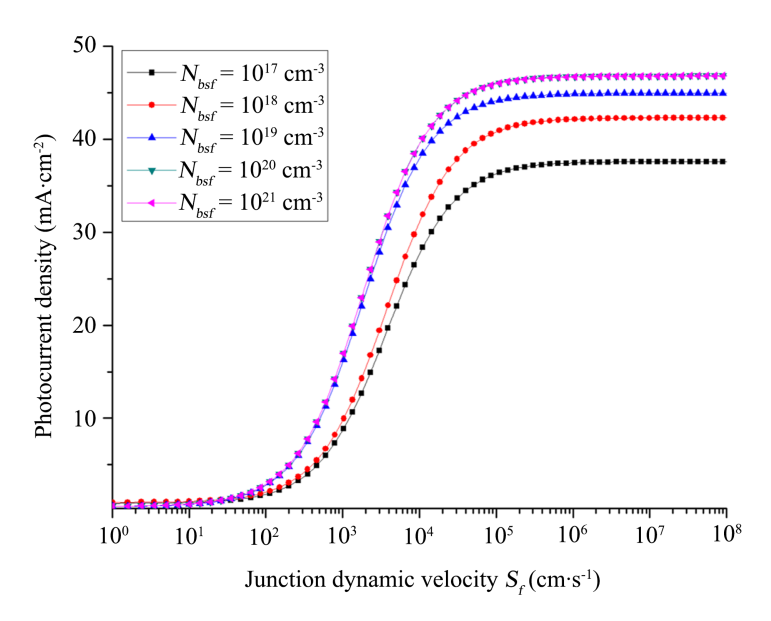


**Figure 8.** The photocurrent density as a function of the dynamic speed at the junction for different doping rates of the overdoped zone p<sup>+</sup> ( $N_b = 10^{16}$  cm<sup>-3</sup>,  $N_e = 10^{19}$  cm<sup>-3</sup>, W = 0.1  $\mu$ m,  $H = 100 \mu$ m,  $W_{bsf} = 0.1 \mu$ m).

For values of  $S_f \le 10^2$  cm·s<sup>-1</sup>, the doping rate of the zone p<sup>+</sup> has no impact on the photocurrent density. On the other hand, for values of  $S_r > 10^2$  cm·s<sup>-1</sup> we have an increase in the photocurrent density. In short circuit, when the doping rate of the overdoped zone p<sup>+</sup> increases from  $10^{17}$  cm<sup>-3</sup> to  $10^{21}$  cm<sup>-3</sup>, an increase in the photocurrent density of approximately 24.52% is observed. This increase is due to the presence of the electric field on the rear surface of the PV cell. Consequently, the minority carriers (electrons) generated near the surface escape the recombination process at the back face [16]. Indeed, the presence of the back electric field of the PV cell makes it possible to minimize recombinations although the doping rate of this zone is high. we can say that the increase in impurities in this area leads to an increase in the photocurrent density at the back face of the PV cell. Now, we will show the impact of the doping rate of the overdoped zone on the photovoltage.

# 5.8. Impact of the Doping Rate of the Overdoped Zone $p^{\scriptscriptstyle +}$ on the Photovoltage

In **Figure 9**, we present the photovoltage curve as a function of the dynamic velocity at the junction for different doping rates of the overdoped zone under simultaneous illumination on both faces.

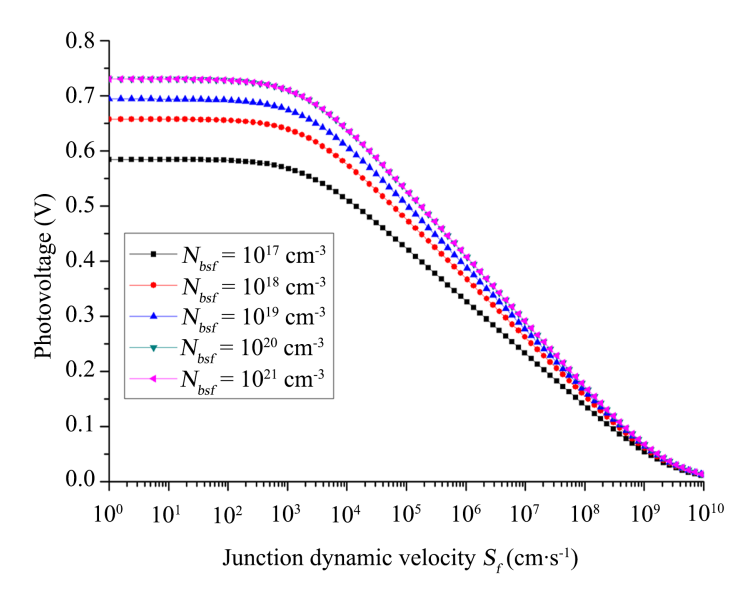


**Figure 9.** Photovoltage as a function of dynamic velocity at the junction for different doping rates overdoped zone p<sup>+</sup> ( $N_b = 10^{16}$  cm<sup>-3</sup>,  $N_e = 10^{19}$  cm<sup>-3</sup>, W = 0.1 μm, H = 100 μm,  $W_{bsf} = 0.1$  μm).

We see an increase in photovoltage when the doping rate increases in the open circuit. Indeed, we see an increase in the photovoltage up to  $N_{bsf} = 10^{20}$  cm<sup>-3</sup> then it remains constant from this value. When the doping rate of the zone increases from  $10^{17}$  cm<sup>-3</sup> to  $10^{21}$  cm<sup>-3</sup>, it appears an increase of about 25% in the open circuit photovoltage. Indeed, the doping rate of the overdoped zone will impact the back electric field (Back Surface Field) which is directed from the base towards this overdoped zone. The potential barrier induced by the difference in doping level between the base and the overdoped zone therefore tends to confine the minority carriers in the base [15]. However, very high doping of the overdoped zone reduces this potential barrier due to the BGN band gap narrowing phenomenon [17]. So the dopant atoms become negative ions at the base-zone interface increasing. Hence an increase in photovoltage. The evolution of the electrical power as a function of the doping rate of the overdoped zone is analyzed in the following part.

# 5.9. Impact of the Doping Rate of the Overdoped Zone p+ on Electrical Power

To determine the behavior of the electrical power as a function of the doping rate of the overdoped zone  $p^+$ , we represent the evolution of the electrical power as a function of the doping rate of the overdoped zone  $p^+$ . The evolution obtained for simultaneous illumination is presented in **Figure 10**.

We observe in Figure 10 that the electrical power by the PV cell is almost zero in the vicinity of the open circuit and the short circuit; it reaches its maximum at an intermediate operating point. For this mode of operation, when the doping rate increases from  $10^{17}$  cm<sup>-3</sup> to  $10^{20}$  cm<sup>-3</sup>, the electrical power increases and then remains constant from  $10^{20}$  cm<sup>-3</sup>. This increase is explained by the increase in the

intensity of the eclectic field. This prevents recombination at the back side of the PV cell. This observation was made at the level of the photovoltage density. In **Table 3** the values of the fill factor are recorded for different values of the doping rate of the overdoped zone.

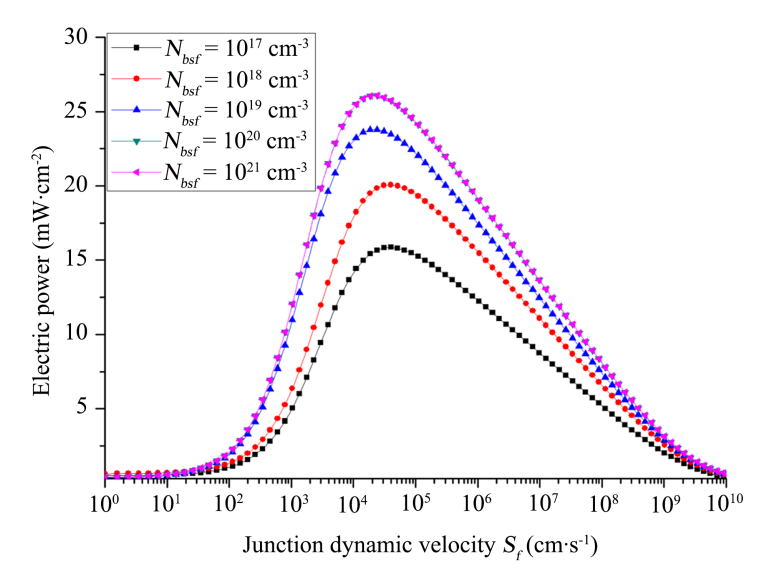


**Figure 10.** Electrical power as a function of dynamic velocity at the junction for different doping rates overdoped zone p<sup>+</sup> ( $N_b = 10^{16}$  cm<sup>-3</sup>,  $N_e = 10^{19}$  cm<sup>-3</sup>, W = 0.1 μm, H = 100 μm,  $W_{bsf} = 0.1$  μm).

**Table 3.** Values of the fill factor as a function of the doping rate  $N_{bsf}$ .

$N_{bsf}$ (cm <sup>-3</sup> )	$P_{\rm max}\left({\rm mW/cm^2}\right)$	$V_{co}\left(\mathrm{mV}\right)$	$J_{cc}$ (mA/cm <sup>2</sup> )	FF(%)
1017	15.68	584.77	37.60	71.31
$10^{18}$	19.85	657.87	42.30	71.33
1019	23.79	694.41	44.97	76.18
$10^{20}$	26.09	730.97	46.84	76.20
1021	26.08	730.98	46.82	76.20

We notice that increasing the doping rate of the overdoped zone  $p^+$  gives a significant improvement in all the parameters of the PV cell until reaching a constant value, but the fill factor remains constant from this value. Indeed, recombination in the overdoped zone  $p^+$  is very weak given its location on the back face of the cell. In addition, the heavily doped overdoped zone  $p^+$  makes it possible to reduce recombination at the semiconductor metal contact. Thus, the optimal doping rate value  $N_{bsf}$  should be within the interval  $[10^{20} \text{ cm}^{-3} - 10^{21} \text{ cm}^{-3}]$ .

#### 6. Conclusions

We determined the impacts of the doping rate on the electrical parameters of the three zones of the bifacial PV cell. It appears that the photocurrent density decreases when the doping rate,  $N_e$  and  $N_b$ , increases. However, the photovoltage increases. On the other hand, these two quantities increase when the doping rate N<sub>bsf</sub> increases. The optimal values of the doping rates of each zone according to the results obtained are as follows:  $N_e = [10^{18} - 10^{19} \text{ cm}^{-3}]$  for the emitter,  $N_b = [10^{16} - 10^{17} \text{ cm}^{-3}]$  for the base,  $N_e = [10^{20} - 10^{21} \text{ cm}^{-3}]$  for the overdoped zone p<sup>+</sup>. It is therefore necessary to take these values into account for an efficient bifacial PV cell.

Furthermore, future investigations should explore the potential impact of recombination at grain boundaries and other environmental factors to further refine our understanding of photovoltaic cell performance.

# Acknowledgements

The authors thank the International Scientific Program (ISP), which through the BUF 01 project, supports their research work.

#### **Conflicts of Interest**

The authors declare no conflicts of interest regarding the publication of this paper.

#### References

- [1] Barro, F., Sané, M. and Zouma, B. (2015) Theoretical Investigation of Base Doping and Illumination Level Effects on a Bifacial Silicon Solar Cell. *British Journal of Applied Science & Technology*, **7**, 610-618. <a href="https://doi.org/10.9734/bjast/2015/15628">https://doi.org/10.9734/bjast/2015/15628</a>
- [2] Konate, R., Zouma, B., Savadogo, M., Barro, F.I., Zerbo, I., Zoungrana, M., et al. (2023) Impacts of the Base and Emitter Doping Rate on the Internal Quantum Efficiency. AIP Conference Proceedings, 3040, Article 070009. https://doi.org/10.1063/5.0177051
- [3] Zouma, B., Maiga, A., Dieng, M., Zougmore, F. and Sissoko, G. (2009) 3d Approach of Spectral Response for a Bifacial Silicon Solar Cell under a Constant Magnetic Field. *Global Journal of Pure and Applied Sciences*, 15, 117-124. <a href="https://doi.org/10.4314/gipas.v15i1.44908">https://doi.org/10.4314/gipas.v15i1.44908</a>
- [4] Dugas, J. and Oualid, J. (1987) 3d-Modelling of Polycrystalline Silicon Solar Cells. Revue de Physique Appliquée, 22, 677-685. <a href="https://doi.org/10.1051/rphysap:01987002207067700">https://doi.org/10.1051/rphysap:01987002207067700</a>
- [5] Dugas, J. (1976) 3D Modelling of a Reverse Cell Made with Improved Multicrystalline Silicon Wafers. Solar Energy Materials and Solar Cells, 32, 71-88. <a href="https://doi.org/10.1016/0927-0248(94)90257-7">https://doi.org/10.1016/0927-0248(94)90257-7</a>
- [6] Lunin, O. and Mathur, S.D. (2002) ADS/CFT Duality and the Black Hole Information Paradox. Nuclear Physics B, 623, 342-394. <a href="https://doi.org/10.1016/s0550-3213(01)00620-4">https://doi.org/10.1016/s0550-3213(01)00620-4</a>
- [7] Rajkanan, K., Singh, R. and Shewchun, J. (1979) Absorption Coefficient of Silicon for Solar Cell Calculations. *Solid-State Electronics*, 22, 793-795.
   <a href="https://doi.org/10.1016/0038-1101(79)90128-x">https://doi.org/10.1016/0038-1101(79)90128-x</a>
- [8] Mohammad, S.N. (2004) An Alternative Method for the Performance Analysis of Silicon Solar Cells. *Journal of Applied Physics*, 61, 767-772. https://doi.org/10.1063/1.338230
- [9] Liou, J.J. and Wong, W.W. (1992) Comparison and Optimization of the Performance

- of Si and Gaas Solar Cells. *Solar Energy Materials and Solar Cells*, **28**, 9-28. https://doi.org/10.1016/0927-0248(92)90104-w
- [10] Swirhun, S.E., Kwark, Y.-. and Swanson, R.M. (1986) Measurement of Electron Lifetime, Electron Mobility and Band-Gap Narrowing in Heavily Doped P-Type Silicon. 1986 *International Electron Devices Meeting*, Los Angeles, 7-10 December 1986, 24-27. https://doi.org/10.1109/jedm.1986.191101
- [11] Bensmaïne, S. and Benyoucef, B. (1999) Analyse des Paramètres Optimaux sur les Microtechnologies Utilisées dans la Fabrication des Cellules Photovoltaïques a Base de Silicium Monocristallin. *REV Renewables & Storage*, 55-64.
- [12] Konate, R., Zouma, B., Ouedraogo, A., Korgo, B., Zoungrana, M. and Kam, S. (2022) Impact of the Thicknesses of the P and P+ Regions on the Electrical Parameters of a Bifacial PV Cell. *Energy and Power Engineering*, 14, 133-145. <a href="https://doi.org/10.4236/epe.2022.142006">https://doi.org/10.4236/epe.2022.142006</a>
- [13] Zoungrana, M., Zerbo, I., Ouédraogo, F., Zouma, B. and Zougmoré, F. (2012) 3D Modelling of Magnetic Field and Light Concentration Effects on a Bifacial Silicon Solar Cell Illuminated by Its Rear Side. *IOP Conference Series: Materials Science and Engineering*, 29, Article 012020. <a href="https://doi.org/10.1088/1757-899x/29/1/012020">https://doi.org/10.1088/1757-899x/29/1/012020</a>
- [14] Samb, M.L., Zoungrana, M., Sam, R., *et al.* (2010) Etude en modelisation a 3-d d'une photopile au silicium en regime statique placee dans un champ magnetique et sous eclairement multispectral: determination des parametres electriques. *Journal des Sciences*, **10**, 23-38.
- [15] Goetzberger, A., Knobloch, J. and Voss, B. (1998) Crystalline Silicon Solar Cell. Institute for Solar Energy Systems.
  <a href="https://api.semanticscholar.org/CorpusID:137390209">https://api.semanticscholar.org/CorpusID:137390209</a>
- [16] Helmaoui, A. (3007) Amelioration du rendement de collecte et la tension Vco. *Revue des Energies Renouvelables*, **2007**, 153-156.
- [17] Godewski, M.P., Baraona, C.R. and Brandhorst, H.W. (1990) Low-High Junction Theory Applied to Solar Cells. Solar Cells, 29, 131-150.